ARTICLES
PUBLISHED ONLINE: 29 JUNE 2015 | DOI: 10.1038/NPHYS3373
nature physics

Translation correlations in anisotropically scattering media

Benjamin Judkewitz[1,2*†], Roarke Horstmeyer[2†], Ivo M. Vellekoop[3], Ioannis N. Papadopoulos[1] and Changhuei Yang[2]

Controlling light propagation across scattering media by wavefront shaping holds great promise for a wide range of communications and imaging applications. But, finding the right shape for the wavefront is a challenge when the mapping between input and output scattered wavefronts (that is, the transmission matrix) is not known. Correlations in transmission matrices, especially the so-called memory effect, have been exploited to address this limitation. However, the traditional memory effect applies to thin scattering layers at a distance from the target, which precludes its use within thick scattering media, such as fog and biological tissue. Here, we theoretically predict and experimentally verify new transmission matrix correlations within thick anisotropically scattering media, with important implications for biomedical imaging and adaptive optics.

Focusing light through strongly scattering media is an important goal in optical imaging and communication. Long considered impossible, recent advances in the field of wavefront shaping[1,2] changed this view by demonstrating that diffuse light can be focused through inhomogeneous media—as long as the correct input wavefront is used. With direct optical access to the target plane, the correct wavefront can be obtained by iterative optimization[2], phase conjugation[3], or by measuring the transmission matrix[4,5]. In many imaging scenarios, however, there is no direct access to the target plane. In those cases, nonlinear[6], fluorescent[7], kinematic[8,9], acousto-optic[10–12] and photo-acoustic[13–15] guide stars can be used as reference beacons. However, these techniques provide wavefront information for only one target location at a time. Although transmission matrices can be sampled quickly with a photo-acoustic approach[16], this method requires absorbing samples. As a result, many samples' transmission matrices can be sampled only sparsely. Correlations within a transmission matrix can compensate for sparse sampling and could enable high-speed imaging. One of the most widely known transmission matrix correlations is the so-called 'memory effect'[17,18], which describes the following phenomenon: when an input wavefront reaching a diffusing sample is tilted within a certain angular range, the output wavefront is equally tilted, resulting in the translation of the far-field speckle pattern at a distance behind the sample (see Fig. 1).

The translation distance within which this effect holds (that is, the field of view (FOV)) is inversely proportional to diffuser thickness L and directly proportional to the distance s of the diffuser from the screen. It can be approximated by the equation $\mathrm{FOV} \approx s\lambda/\pi L$ (refs 19–22).

The memory effect has found numerous applications for point scanning[23,24], direct image transfer[20] and for computational image recovery[21,22,25,26]. Yet, in all of these applications, the target plane was at a distance from a thin diffuser with free space in between ($s > 0$)—which has limited use for imaging inside thick scattering media. As such samples are neither thin nor at a distance from the target area of interest, the correlations predicted by the 'traditional' memory effect should be minimal[27]. Here, we set out to examine whether there are other correlations that apply to such samples. We show that significant transmission correlations can exist in thick scattering media at zero distance, as long as scattering is directional.

Traditional memory effect

Although the memory effect has been extensively derived from first principles[18], these derivations relied on assuming perfectly diffuse scattering–which does not apply to many biological samples. Here we will approach the problem without relying on diffusion, but instead using transmission matrices. Specifically, we are interested in the matrix $T_x = T(x_a, x_b)$, which defines the relationship between the spatial input and output optical modes of a scattering slab (that is, from input plane A to output plane B). For simplicity of graphical representation, we assume propagation of one-dimensional (1D) wavefronts in a 2D geometry, but all conclusions will be generalizable to 2D wavefronts in a 3D geometry. Owing to its discrete nature, the transmission matrix is especially amenable to experimental observation. We will first use our framework to analyse the traditional memory effect, and then calculate the speckle correlations in thick anisotropic media.

When assuming highly randomizing transmission, but incomplete measurement of input and output channels, the transmission matrix is often modelled as a random matrix with complex Gaussian elements. However, the transmission matrix will have an additional macroscopic structure, which will be particularly prominent for thin scattering slabs: a point source on the input plane of the slab would spread to a diffuse spot at the output plane (whose diameter would be of the order of L for slabs with thickness L larger than one transport mean free path—as predicted by the diffusion approximation). As a result, even though individual transmission matrix elements may not be known, the average amplitudes of the transmission matrix elements decrease with distance from the diagonal. The

[1]Exzellenzcluster NeuroCure, Charité Berlin, Humboldt University, Charitéstr. 1, 10117 Berlin, Germany. [2]California Institute of Technology, Departments of Electrical and Bioengineering, 1200 E California Boulevard, Pasadena, California 91125, USA. [3]MIRA Institute for Biomedical Technology and Technical Medicine, University of Twente, PO Box 217, 7500 AE Enschede, Netherlands. †These authors contributed equally to this work.
*e-mail: benjamin.judkewitz@charite.de

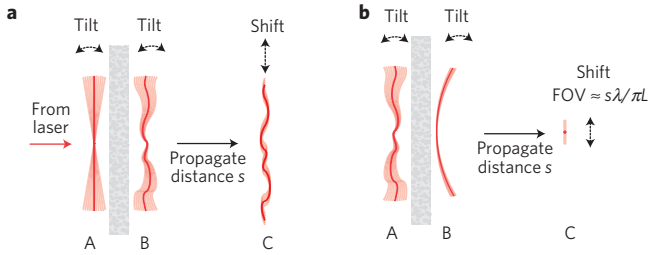

Figure 1 | The traditional memory effect. a, The traditional memory effect as described for light propagating through thin diffusing slabs. Tilting the input wavefront (plane A) reaching the slab tilts the scattered wavefront at the output (plane B), which shifts the far-field intensity speckle pattern projected on a screen (plane C). **b**, When the input wavefront is shaped to converge at a spot on the screen, tilting the input wavefront scans the spot laterally, which can be used for imaging by point scanning. The FOV of this approach is approximated by the equation $\mathrm{FOV} \approx s\lambda/\pi L$.

corresponding bell-shaped profile along each transmission matrix column turns T_x into a band matrix (see Fig. 2a).

To recognize tilt correlations, we are interested in how the band structure of T_x manifests itself in the spatial frequency domain (k-space) representation. Every spatial-domain transmission matrix T_x can the transformed into the corresponding frequency-domain transmission matrix $T_k = T(k_a, k_b)$ by the following operation: $T_k = FT_xF^{-1}$, where F is a discrete Fourier transform matrix. Here, k_a and k_b are wavevectors at the input and output surfaces, respectively. This operation is analogous to performing a 2D Fourier transform and flipping it horizontally (we denote these two operations by the operator $\mathcal{F}_{2D}$):

$$T_k \propto \mathcal{F}_{2D} T_x \tag{1}$$

Expressing T_k in terms of the 2D Fourier transform of T_x provides a straightforward explanation of how the macroscopic structure of T_x influences correlations in T_k. Large values within T_x will tend to concentrate near its diagonal, and entries will be zero elsewhere. As T_x is narrow across the diagonal, its flipped 2D Fourier transform (equation (1)) will contain features that are elongated along the diagonal. The resulting diagonal correlations in T_k correspond to the traditional memory effect, in which a tilt of the input wavefront (shift in k-space) causes a tilt of the output wavefront, resulting in a shifted speckle pattern at a distant screen. For this reason, and to distinguish the traditional memory effect from further correlations described below, we also refer to the traditional memory effect as a 'tilt/tilt correlation'.

The band structure of T_x can be described analytically with a spatial intensity propagator matrix[28]: $P_x(x_a, x_b) \equiv \langle |T_x(x_a, x_b)|^2 \rangle$. This ensemble average removes any statistical fluctuations in T_x. The average spread of intensity across the output surface, from illumination with a point source input, will manifest itself in P_x as a non-negative envelope along its near-diagonals. The cross-correlation theorem may then help re-express the spatial intensity propagator matrix in the frequency domain:

$$\mathcal{F}_{2D}^{x\to\Delta k} P_x = \Sigma_{k_a,k_b} \langle T_k(k_a,k_b) T_k^*(k_a - \Delta k_a, k_b - \Delta k_b) \rangle$$
$$\propto C_k(\Delta k_a, \Delta k_b) \tag{2}$$

Here, $C_k(\Delta k_a, \Delta k_b)$ is the tilt/tilt correlation function, and $\Delta k_a = k_a - k_a'$ and $\Delta k_b = k_b - k_b'$ denote shifts in input and output wavevectors, respectively. Typically, it is assumed that, P_x depends only on the difference between the input and output spatial coordinates (shift-invariance). Then, equation (2) simplifies to

$$C_k(\Delta k_a, \Delta k_b) \propto \delta_{\Delta k_a, \Delta k_b} \mathcal{F}^{\Delta x \to \Delta k_b} P_x(\Delta x) \tag{3}$$

where $\Delta x = x_b - x_a$ and δ is a Kronecker delta. Equation (3) is the well-known memory effect[28]. As can be seen directly from equation (2), the angular range over which the memory effect is significant is inversely proportional to the width of the intensity propagator, P_x. When considering intensity transmission, equation (3) corresponds to the lowest-order $C^{(1)}$ term[18]. Unlike such prior work, equation (2) also describes the general case of tilt/tilt correlations for a geometry that is not invariant under lateral translation.

These considerations reconfirm our expectation that the traditional memory effect may be minimal in thick biological media. First, the average spread of intensity from the input to output surface will increase with sample thickness, L (ref. 29). A wider $P_x(\Delta x)$ will subsequently reduce the range of tilt/tilt correlations between the input and output planes. Second, the plane of interest is not at a distance from the sample, which means that the tilt at the output plane would not translate into a useful spatial shift at the target plane.

Correlations in anisotropic media

We therefore investigated whether there might be other types of transmission matrix correlation in thick samples, such as biological media. We started by recognizing that in many samples scattering is anisotropic and occurs primarily in the forward direction. Scattering is particularly anisotropic in biological media, where the anisotropy parameter g (the average cosine of the scattering angle) typically ranges from 0.9 to 0.98 (refs 30,31). This means that after a limited number of scattering events, the directionality of an input beam will be preserved to some extent as it reaches the output plane. In other words, one input plane wave (one mode in k-space) will result in a limited angular span of output waves.

As a result of such preserved directionality, anisotropically scattering media will have a macroscopic structure in the T_k matrix (rather than T_x). Large amplitudes in T_k will primarily concentrate near its main diagonal (see Fig. 2b). By analogy to our prior reasoning for the traditional memory effect, if T_k is a band matrix, the entries within each diagonal of its associated T_x will be correlated with one another. Now, a spatial shift of the optical field at the input plane will cause a spatial shift of the field at the output plane (this is in contrast to the traditional memory effect, in which a tilt at the input plane causes a tilt at the output plane).

The range of correlations in T_x will depend on the width of the diagonally bordered envelope in T_k. Equivalent to equation (2), we may define a k-space intensity propagator using an ensemble average: $P_k(k_a, k_b) \equiv \langle |T_k(k_a, k_b)|^2 \rangle$. Here, the average intensity spread of each input plane wave into a finite output wavevector 'cone' now specifies the envelope shape along the columns of P_k. Following equation (3), we may show that the band structure of P_k creates correlations in space:

$$\mathcal{F}_{2D}^{k\to\Delta x} P_k = \Sigma_{x_a,x_b} \langle T_x(x_a,x_b) T_x^*(x_a - \Delta x_a, x_b - \Delta x_b) \rangle$$
$$\propto C_x(\Delta x_a, \Delta x_b) \tag{4}$$

with $C_x(\Delta X_a, \Delta X_b)$ being the shift/shift correlation function. If the k-space propagator P_k depends only on difference coordinates, then equation (4) reduces to

$$C_x(\Delta x_a, \Delta x_b) \propto \delta_{\Delta x_a, \Delta x_b} \mathcal{F}^{\Delta k \to \Delta x_b} P_k(\Delta k) \tag{5}$$

where $\Delta k = k_b - k_a$. This result predicts the existence of shift/shift correlations that are the exact Fourier conjugate of the traditional (tilt/tilt) memory effect.

In equation (5), P_k includes the effects of sample anisotropy. Its width scales inversely proportional with g but will increase with sample thickness L (see Supplementary Section C). If P_k depends only on difference coordinates, the correlation function can be

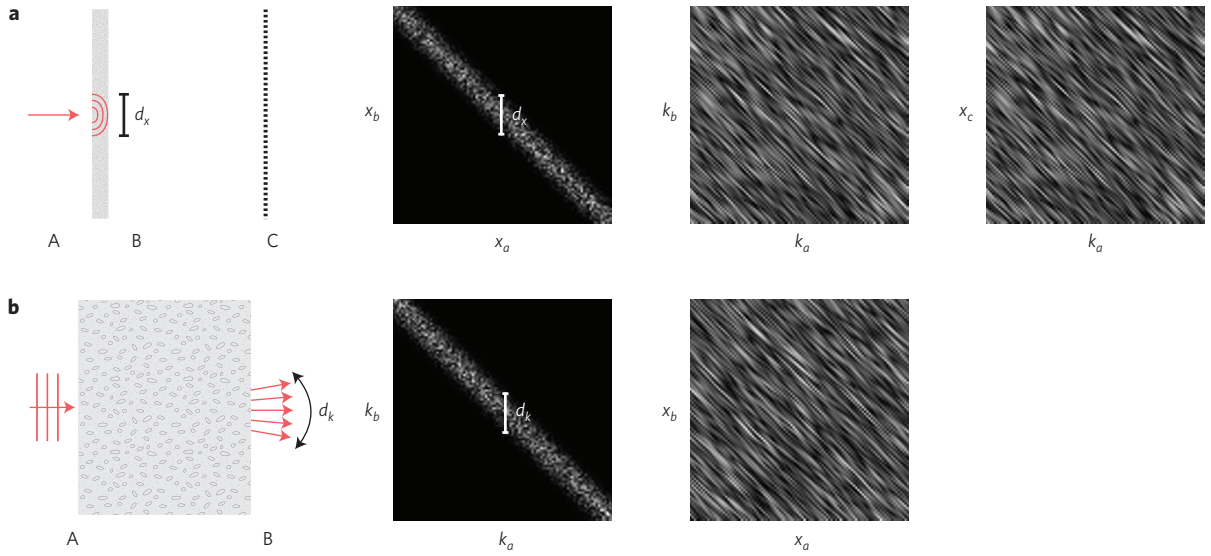

Figure 2 | Correlations within transmission matrices (simulated). a, The traditional (tilt/tilt) memory effect explained in terms of transmission matrix correlations. A pencil beam illuminating a thin slab will cause a diffuse spot at the output surface, whose diameter d_X is of the order of the slab thickness L. The profile of the spot will be apparent in the (ordered) X/X transmission matrix, and results in strong near-diagonal components and zeros elsewhere. The corresponding K/K transmission matrix is diagonally smeared (because X/X and K/K transmission matrices are related by the 2D Fourier transform). Hence, a tilt (k-shift) at the input plane results in a corresponding tilt (k-shift) at the output plane. **b**, In anisotropically scattering media of finite thickness, the directionality of the input light may be preserved. As a result, a plane wavefront illuminating the sample creates a limited spread of output wavefronts, d_K. This suggests that the K/K transmission matrix of anisotropic samples has elements of higher magnitude near its diagonal. This results in a diagonally smeared X/X transmission matrix, indicating shift/shift correlations.

predicted by a simple experiment, namely by illuminating the sample with a plane wave $E_p(x_a) = 1$ and measuring the output wavefront, $E_p(x_b) = T_x E_p(x_a)$. The spectrum of $E_p(x_b)$ indicates the average spread of wavevectors exiting the output surface:

$$P_k(\Delta k) \equiv |\mathcal{F}^{x_b \to \Delta k} E_p(x_b)|^2 \quad (6)$$

The Fourier transform of equation (6) subsequently yields the correlation between the electric field outputs from two spatially shifted inputs. In effect, the shape of the shift/shift correlation function equals the autocorrelation of $E_p(x_b)$. A more detailed derivation of equations (1)–(6) can be found in the Supplementary Information.

Experimental validation

To validate our predictions experimentally, we created four scattering samples with well-defined scattering properties (3-μm-diameter silica beads dispersed in agarose gel, $g = 0.978$ as calculated by Mie theory and scattering length $1/\mu_s = 175\,\mu$m at 632 nm, slab thickness L in micrometres: 140, 280, 560 and 1,120, or 1, 2, 4 and 8 spacers of 140 μm thickness). We then performed four different experiments with this scattering sample set, as detailed below.

First, we illuminated each sample with a random input wave and recorded the output field, E_0, using off-axis digital holography. We translated each sample laterally (Δx ranging from $-10\,\mu$m to $10\,\mu$m in 0.2 μm steps) and measured the absolute correlation $C(\Delta x)$ between the resulting output fields, $E_{\Delta x}$, and E_0: $C(\Delta x) = \mathrm{corr}(E_0, E_{\Delta x})$ (Fig. 3a,c). Second, to compare these results with our predictions in equation (6), we illuminated each of the samples with a plane wave and calculated the autocorrelation of the output speckle patterns (Fig. 3b,d). Third, our theory predicts that the correlation function for one sample thickness L_0 can be used to estimate the correlation function for any other thickness (see Supplementary Equation C3); for example, the correlation function for a slab of thickness $2L_0$ is simply the correlation function for a slab of thickness L_0, squared. We therefore used the speckle autocorrelation measured for the thinnest slab (blue curve in Fig. 3d) and calculated the remaining correlation functions using Supplementary Equation C4 (Fig. 3e). Fourth, we used Mie theory to obtain a single-scattering phase function for our bead samples, and calculated the theoretical correlation function using Supplementary Equation C1 (Fig. 3f). We computed this last set of curves using only the refractive indices of the media, the bead diameter and slab optical thickness (that is, without using experimental data), as detailed in Supplementary Section C. Figure 3f combines all four strategies for determining the correlation function into one plot. It illustrates that the experimentally measured correlation function is in agreement with all three of our derived predictions.

The shift/shift correlations apply to any input field, including fields that are shaped to converge to a sharp focus. To demonstrate the use of these correlations for scanning a point focus across a biological sample, we first used optical phase conjugation[3] to focus light (780 nm diode laser) through 500-μm- to 1-mm-thick slices of chicken muscle tissue, employing off-axis holography for wavefront measurement and a spatial light modulator (SLM) for wavefront shaping[11,12] (Fig. 4a). We projected a point source at one surface of the tissue slice (surface A) and detected the scattered wavefront propagating from this point through the tissue (exiting at surface B) to the SLM plane. In the next step, we displayed the phase conjugate of the detected wavefront, which travelled back through the tissue and formed a focus on surface A.

To validate the predicted shift/shift correlations, we then shifted the phase-conjugated wavefront laterally at surface B, testing whether the focus at surface A would be preserved and whether it moved. As expected, we noticed that motion of the shaped wavefront resulted in concurrent movement of the focus (Fig. 4b,c), while the focus intensity decreased with distance from the original position, following a bell-shaped curve (Fig. 4d,e). For the 500 μm slice the full-width at half-maximum (FWHM) was 5 μm, and the full-width at tenth-maximum (FWTM) was 10 μm. In the case of the 1,000 μm slice, the FWHM was 3 μm and the FWTM was 6 μm.

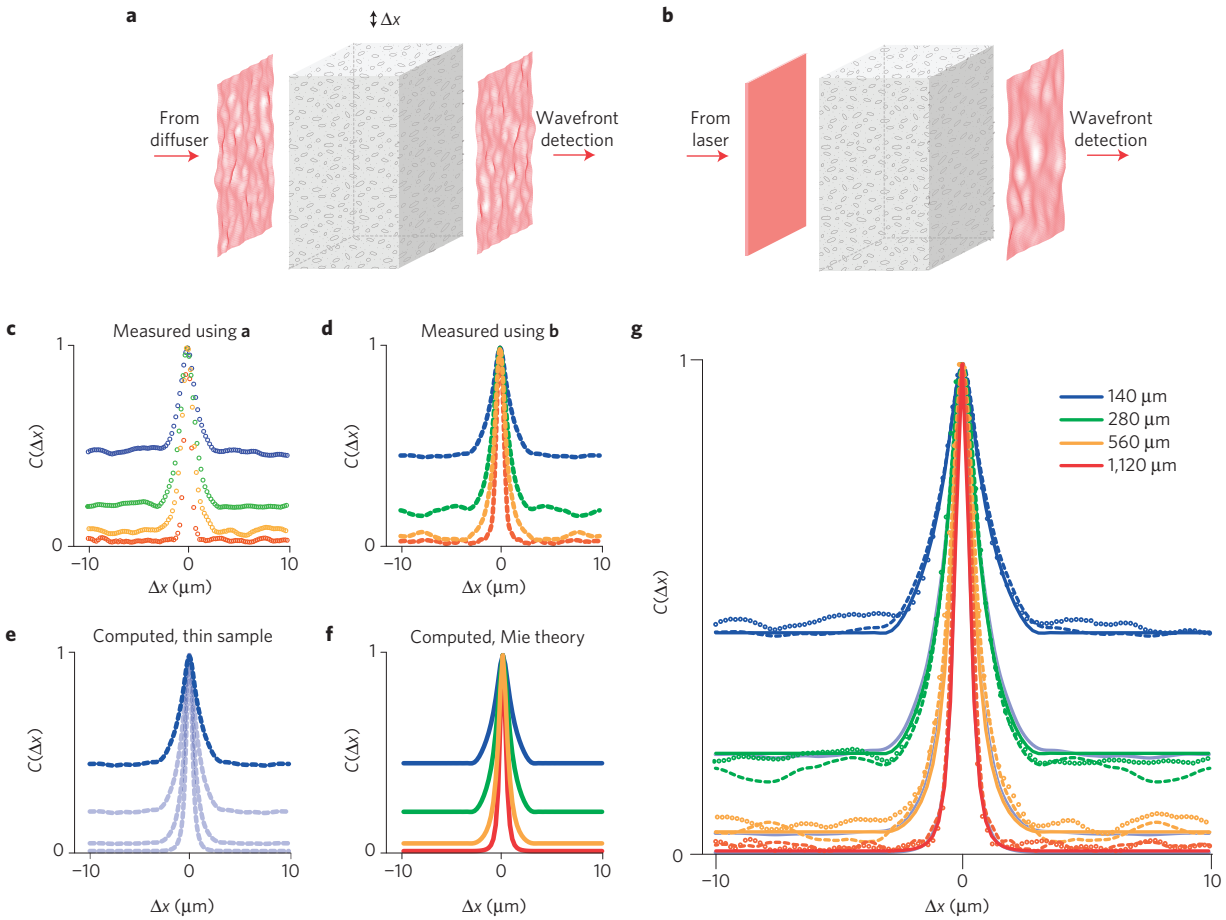

Figure 3 | Experimental validation. a, Experimental set-up for determining the shift/shift field correlation, $C(\Delta x)$, directly. **b**, Experimental set-up for determining $C(\Delta x)$ using the speckle autocorrelation resulting from plane-wave illumination. **c**, Experimentally measured $C(\Delta x)$ using the set-up in **a**. **d**, $C(\Delta x)$ obtained from the speckle autocorrelations measured in **b**. **e**, Correlation functions calculated from the speckle autocorrelation for the thinnest sample (blue line in **d**). **f**, Correlation functions predicted by the radiative transfer equation using a phase function obtained by Mie theory. **g**, Overlay. We made samples with different thicknesses to cover a range of the forward-scattering and quasi-ballistic regime. As the thinnest sample is thinner than $1/\mu_s$, the constant background in the correlations is due to the fact that speckles are not yet fully developed. As the thickness of the samples increases, and speckles get more developed, the constant background approaches zero.

Published scattering parameters for chicken tissue vary, and owing to experimental limitations, the single-scattering phase function has not been determined. However, equation (6) provides a practical way to predict the shift/shift correlation function from the experimentally accessible speckle autocorrelation function. We therefore illuminated the samples with a plane wavefront and examined whether the shape of the spatial autocorrelation of the resulting speckle pattern followed the profile of the shift/shift correlations (C_x), as derived in equation (6). Indeed, Fig. 4d,e shows that both profiles are in good experimental agreement.

Discussion

The traditional (tilt/tilt) memory effect has recently enabled the development of several modalities to image through scattering 'walls'[20–26]. Intriguing as these methods are, they suffer from two limitations: the sample should be thin, and the object should be placed at a distance behind the sample.

Here, we demonstrated a complementary type of memory effect that suffers from neither limitation: the correlations are present even inside thick scattering media, as long as scattering is anisotropic and the mapping between input and output wavefronts preserves any level of directionality. This is the case up to a depth of about one transport mean free path.

We showed that the shift/shift memory effect is the Fourier complement of the traditional (tilt/tilt) memory effect, and that the extent of correlations can be directly determined from the spatial speckle autocorrelation function during plane-wave illumination.

Our theory is general in the sense that it applies to any linear propagation, which can be described by an input–output matrix. If this matrix is banded in the spatial frequency domain, there will be shift/shift correlations. This means that there will be an effect whenever the directionality of the input waves is maintained to some degree at a chosen output plane, where the 'output' plane could be inside the sample, on the opposite surface, or beyond the opposite surface in free space.

As compared with correlations measured at the surface, the extent of correlations within biological media may be affected by diffuse back-scattering from deeper layers. To estimate the extent of this effect, we can decompose the angular intensity propagator P_k into the forward-scattered component (equivalent to the one measured at the output surface of a slab with thickness t) and the back-scattered or diffuse component. In the case of highly anisotropic media such as biological tissue, we can expect that the forward-propagating component will dominate in the quasi-ballistic regime. For example, if the ratio of back-scattered versus forward-scattered power in the semi-infinite medium at depth t was 20%, we would

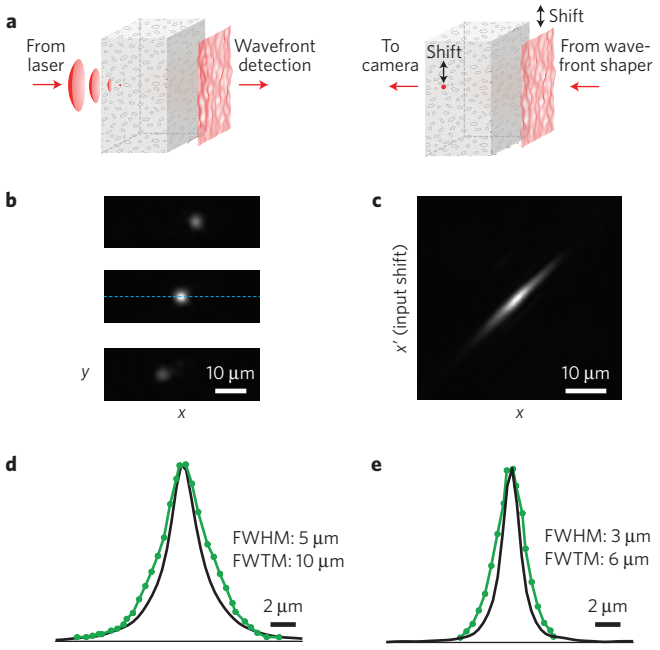

Figure 4 | Using shift/shift correlations for focusing. a, Experimental set-up. **b**, The time-reversed spot (middle) and shifted foci resulting from laterally shifting the phase-conjugated wavefront at the sample. **c**, Line scan (intensity profile) along the blue dashed line in **b** while shifting the input wavefront. **d**,**e**, Focus peak intensity as a function of shifted location for 500 μm (**d**) and 1,000 μm (**e**) tissue slices. Black curve: prediction based on the speckle autocorrelation measured during plane-wave illumination (equation (2)).

still expect 80% of the field correlations present at the surface of an equivalent slab with thickness t.

Thus, our results pave the way for extending memory-effect-based imaging methods[20–26] to also work inside biological tissue. On the basis of our measurements, we expect such methods to achieve diffraction-limited resolution at a depth of 1 mm inside muscle tissue, albeit at a limited FOV of <10 μm, initially.

We foresee several possibilities to further increase the FOV of our method, for example by tiling neighbouring FOVs using multiple corrections or by interpolating a sparsely sampled transmission matrix, which can be under-sampled by two orders of magnitude. Furthermore, our results suggest that the extent of correlations will be largest for photons that have undergone few scattering events and little angular deviation—also called snake-photons. Hence, selective measurement and correction of snake-photons (for example, by temporal gating, coherence gating or spatial filtering) may considerably increase the extent of correlations and the imaging FOV.

Finally, we note that tilt/tilt and shift/shift correlations are not mutually exclusive. For example, recent work establishes that light within biological tissue exhibits much stronger tilt/tilt correlations than in low-g media[32]. This is because light spreads less across both angle and space in anisotropically scattering media, making both P_k and P_x highly non-uniform. Even though using strict tilt/tilt correlations for scanning or imaging still requires a finite distance between the scattering sample and target (and may thus not be applicable for imaging biological media), we anticipate that a potential combination of both memory effects into a joint model could further extend the translation correlations described here. Furthermore, we anticipate that there may be additional correlations present in biological media. Future work measuring complete transmission matrices in the adaptive optics and the complex wavefront shaping regime will shed light on spectral, temporal and spatial correlations. They may ultimately be used in combination with the shift/shift correlations reported here.

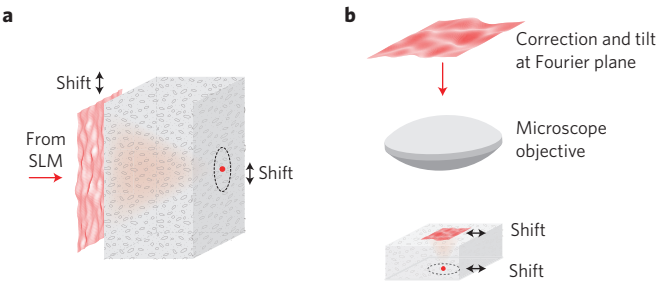

Figure 5 | Comparison between shift/shift correlations and adaptive optics microscopy. a, Shift/shift correlations, in which a point at the target plane can be scanned by shifting the corrected input wavefront. The range of correlations is indicated by the dashed line. **b**, Typical set-up in adaptive optics microscopy, where corrected wavefronts are tilted in the Fourier plane. This leads to a shift of the propagated wavefront at the sample surface, causing a shift of the corrected focus. The so-called isoplanatic patch (that is, the range within which the correction applies) is indicated by the dashed circle.

We note that the described shift/shift correlations are consistent with the set-up geometry of adaptive optics microscopy (Fig. 5), where wavefronts are corrected in the conjugate Fourier plane of the microscope objective. Tilting the incoming wavefront in the Fourier plane (for example, in a laser scanning microscope) leads to a shift of the wavefront reaching the sample and a resulting shift of the focus[33]. In other words, adaptive optics microscopy implicitly already takes advantage of shift/shift correlations, albeit in the ballistic regime—as such it can be interpreted as a special case of the general shift/shift correlations derived here.

With further study of spatial, spectral and temporal transmission matrix correlations, these advances may lead to a unified understanding of adaptive optics and complex wavefront shaping and extend their use in thick biological tissues, enabling versatile imaging and photostimulation in a wide range of biologically relevant media.

Received 24 February 2015; accepted 21 May 2015; published online 29 June 2015

References

1. Mosk, A. P., Lagendijk, A., Lerosey, G. & Fink, M. Controlling waves in space and time for imaging and focusing in complex media. *Nature Photon.* **6,** 283–292 (2012).
2. Vellekoop, I. M. & Mosk, A. P. Focusing coherent light through opaque strongly scattering media. *Opt. Lett.* **32,** 2309–2311 (2007).
3. Yaqoob, Z., Psaltis, D., Feld, M. S. & Yang, C. Optical phase conjugation for turbidity suppression in biological samples. *Nature Photon.* **2,** 110–115 (2008).
4. Popoff, S., Lerosey, G., Fink, M., Boccara, A. C. & Gigan, S. Image transmission through an opaque material. *Nature Commun.* **1,** 81 (2010).
5. Choi, W., Mosk, A. P., Park, Q-H. & Choi, W. Transmission eigenchannels in a disordered medium. *Phys. Rev. B* **83,** 134207 (2011).
6. Hsieh, C-L., Pu, Y., Grange, R. & Psaltis, D. Digital phase conjugation of second harmonic radiation emitted by nanoparticles in turbid media. *Opt. Express* **18,** 12283–12290 (2010).
7. Tao, X. *et al.* Live imaging using adaptive optics with fluorescent protein guide-stars. *Opt. Express* **20,** 15969–15982 (2012).
8. Ma, C., Xu, X., Liu, Y. & Wang, L. V. Time-reversed adapted-perturbation (TRAP) optical focusing onto dynamic objects inside scattering media. *Nature Photon.* **8,** 931–936 (2014).
9. Zhou, E. H., Ruan, H., Yang, C. & Judkewitz, B. Focusing on moving targets through scattering samples. *Optica* **1,** 227–232 (2014).
10. Xu, X., Liu, H. & Wang, L. V. Time-reversed ultrasonically encoded optical focusing into scattering media. *Nature Photon.* **5,** 154–157 (2011).
11. Wang, Y. M., Judkewitz, B., DiMarzio, C. A. & Yang, C. Deep-tissue focal fluorescence imaging with digitally time-reversed ultrasound-encoded light. *Nature Commun.* **3,** 928 (2012).

12. Judkewitz, B., Wang, Y. M., Horstmeyer, R., Mathy, A. & Yang, C. Speckle-scale focusing in the diffusive regime with time reversal of variance-encoded light (TROVE). *Nature Photon.* **7,** 300–305 (2013).
13. Kong, F. *et al.* Photoacoustic-guided convergence of light through optically diffusive media. *Opt. Lett.* **36,** 2053–2055 (2011).
14. Conkey, D. B. *et al.* Super-resolution photoacoustic imaging through a scattering wall. Preprint at http://arXiv.org/abs/1310.5736 (2013).
15. Lai, P., Wang, L., Tay, J. W. & Wang, L. V. Photoacoustically guided wavefront shaping for enhanced optical focusing in scattering media. *Nature Photon.* **9,** 126–132 (2015).
16. Chaigne, T. *et al.* Controlling light in scattering media non-invasively using the photoacoustic transmission matrix. *Nature Photon.* **8,** 58–64 (2014).
17. Freund, I., Rosenbluh, M. & Feng, S. Memory effects in propagation of optical waves through disordered media. *Phys. Rev. Lett.* **61,** 2328–2331 (1988).
18. Feng, S., Kane, C., Lee, P. & Stone, A. Correlations and fluctuations of coherent wave transmission through disordered media. *Phys. Rev. Lett.* **61,** 834–837 (1988).
19. Freund, I. Looking through walls and around corners. *Physica A* **168,** 49–65 (1990).
20. Katz, O., Small, E. & Silberberg, Y. Looking around corners and through thin turbid layers in real time with scattered incoherent light. *Nature Photon.* **6,** 549–553 (2012).
21. Bertolotti, J. *et al.* Non-invasive imaging through opaque scattering layers. *Nature* **491,** 232–234 (2012).
22. Katz, O., Heidmann, P., Fink, M. & Gigan, S. Non-invasive single-shot imaging through scattering layers and around corners via speckle correlations. *Nature Photon.* **8,** 784–790 (2014).
23. Hsieh, C-L., Pu, Y., Grange, R., Laporte, G. & Psaltis, D. Imaging through turbid layers by scanning the phase conjugated second harmonic radiation from a nanoparticle. *Opt. Express* **18,** 20723–20731 (2010).
24. Vellekoop, I. M. & Aegerter, C. M. Scattered light fluorescence microscopy: Imaging through turbid layers. *Opt. Lett.* **35,** 1245–1247 (2010).
25. Yang, X., Pu, Y. & Psaltis, D. Imaging blood cells through scattering biological tissue using speckle scanning microscopy. *Opt. Express* **22,** 3405–3413 (2014).
26. Takasaki, K. T. & Fleischer, J. W. Phase-space measurement for depth-resolved memory-effect imaging. *Opt. Express* **22,** 31426–31433 (2014).
27. Psaltis, D. & Papadopoulos, I. N. Imaging: The fog clears. *Nature* **491,** 197–198 (2012).
28. Li, J. H. & Genack, A. Z. Correlation in laser speckle. *Phys. Rev. E* **49,** 4530–4533 (1994).
29. Berkovits, R., Kaveh, M. & Feng, S. Memory effect of waves in disordered systems: A real-space approach. *Phys. Rev. B* **40,** 737–740 (1989).
30. Jacques, S. L. Optical properties of biological tissues: A review. *Phys. Med. Biol.* **58,** R37–R61 (2013).
31. Cheong, W-F., Prahl, S. A. & Welch, A. J. A review of the optical properties of biological tissues. *IEEE J. Quantum Electron.* **26,** 2166–2185 (1990).
32. Schott, S., Bertolotti, J., Léger, J-F., Bourdieu, L. & Gigan, S. Characterization of the angular memory effect of scattered light in biological tissues. *Opt. Express* **23,** 13505–13516 (2015).
33. Ji, N., Sato, T. R. & Betzig, E. Characterization and adaptive optical correction of aberrations during *in vivo* imaging in the mouse cortex. *Proc. Natl Acad. Sci. USA* **109,** 22–27 (2012).

Acknowledgements

We thank I. Freund, R. Chen and M. Jang for discussions and for providing very helpful feedback on this manuscript. This work was supported by the German Research Foundation, DFG (EXC 257 NeuroCure), NIH 1DP2OD007307-01 and the Wellcome Trust (WT092197MA).

Author contributions

B.J. and R.H. conceived and developed the idea with essential help from I.M.V. B.J. and I.N.P. performed experiments. B.J., R.H. and I.M.V. wrote the manuscript. R.H. and I.M.V. wrote the mathematical supplement with help from B.J. B.J. and C.Y. supervised the project.

Additional information

Supplementary information is available in the online version of the paper. Reprints and permissions information is available online at www.nature.com/reprints. Correspondence and requests for materials should be addressed to B.J.

Competing financial interests

The authors declare no competing financial interests.